# Role of hydrogen in hydrogen-induced layer exfoliation of germanium

J. M. Zahler,[1] A. Fontcuberta i Morral,[1,2] M. J. Griggs,[1] Harry A. Atwater,[1] and Y. J. Chabal[3]
[1]*Thomas J. Watson Laboratory of Applied Physics, California Institute of Technology, Pasadena, California 91125, USA*
[2]*Walter Schottky Institut, Technische Universität München, 85748 Garching, Germany*
[3]*Laboratory for Surface Modification, Rutgers University, Piscataway, New Jersey 08854, USA*
(Received 3 August 2006; revised manuscript received 12 November 2006; published 9 January 2007)

The role of hydrogen in the exfoliation of Ge is studied using cross-sectional transmission electron microscopy, atomic force microscopy, and multiple-internal transmission mode Fourier-transform infrared absorption spectroscopy and compared with the mechanism in silicon. A qualitative model for the physical and chemical action of hydrogen in the exfoliation of these materials is presented, in which H-implantation creates damage states that store hydrogen and create nucleation sites for the formation of micro-cracks. These micro-cracks are chemically stabilized by hydrogen passivation, and upon annealing serve as collection points for molecular hydrogen. Upon further heating, the molecular hydrogen trapped in these cracks exerts pressure on the internal surfaces causing the cracks to extend and coalesce. When this process occurs in the presence of a handle substrate that provides rigidity to the thin film, the coalescence of these cracks leads to cooperative thin film exfoliation. In addition to clarifying the mechanism of H-induced exfoliation of single-crystal thin Ge films, the vibrational study helps to identify the states of hydrogen in heavily damaged Ge. Such information has practical importance for the optimization of H-induced layer transfer as a technological tool for materials integration with these materials systems.

DOI: 10.1103/PhysRevB.75.035309 PACS number(s): 68.55.Ln, 78.30.−j, 68.37.Lp, 68.35.Ja

## I. INTRODUCTION

Hydrogen-induced exfoliation of semiconductors combined with wafer bonding techniques has been applied for more than a decade to the layer transfer of thin films onto nonlattice matched substrates. H-implantation is a technological process that allows the insertion of a hydrogenated layer in a material. $H^+$ ions are accelerated with relatively high voltages (80 keV in our case) and are stopped at a certain distance from the surface, producing damage in the material mainly in the form of vacancies in the matrix. For energetic reasons, the created damage states tend to store hydrogen and create nucleation sites for the formation of micro-cracks. These micro-cracks are believed to be chemically stabilized by hydrogen passivation, and upon annealing serve as collection points for molecular hydrogen. Upon further heating, the molecular hydrogen trapped in these cracks exerts pressure on the internal surfaces causing the cracks to extend and coalesce. When this process occurs in the presence of a handle substrate that provides rigidity to the thin film, the coalescence of these cracks leads to exfoliation. This process was first developed for silicon[1] and is the basis of the industrial production of silicon-on-insulator (SOI) substrates. Wafer bonding and layer transfer has now been applied to semiconductors other than silicon such as Ge, InP, GaAs, and GaN.[2–6] The mechanism of H-induced exfoliation has been extensively studied in the case of silicon,[7,8] and, more recently, in the case of InP.[9] The early work of Weldon *et al.* provided important conclusions: (i) implantation induced defects serve to trap H within the Si substrate. (ii) A broad distribution of vacancy hydrogen defect structures is the main reservoir for hydrogen that contribute to the exfoliation process. For subcritical doses of H, the spectral fingerprint for these vacancies is significantly diminished. (iii) Agglomerated $VH_{3,4}$ defect structures are precursors to the formation of extended internal surfaces that serve to accumulate $H_2$ and build internal pressure. Furthermore, the (100) and (111) platelet structures observed in TEM serve as nucleation points for the agglomeration of vacancy-hydrogen defect structures; (iv) The concentration of bound hydrogen is reduced upon annealing, as indicated by a decrease in the integrated intensity of the Si-H modes. Yet, the majority of hydrogen was shown by forward recoil scattering (FRS) to remain in the Si rather than to diffuse out of the semiconductor. Thus, the loss of bound hydrogen leads to the formation of molecular $H_2$ confined to internal structures. (v) $H_2$ trapped in internal surfaces was shown by mass spectroscopy to have the physical role of pressurizing the micro-cracks to provide the energy necessary for their extension through the material. (vi) By studying bonded implanted samples along with free surfaces, it was shown that the presence of the handle substrate plays only a dynamic role as a stiffener during the internal pressurization of the micro-cracks. This induces lateral crack growth, but shows no spectroscopic difference from the free surface sample.

The H-induced exfoliation mechanism of Ge is expected to be qualitatively similar to this process summarized above for Si. However, the chemical activity of Ge and Si is often quantitatively different. Although the characteristics of isolated H-stabilized defects are similar in Si and Ge,[10,11] it is important to investigate the behavior of high concentration of hydrogen in Ge during the exfoliation process. Such a study is not only important to understand the fundamentals of H-induced layer exfoliation of germanium, but also as a source of reference of the Ge-H related vibrational modes in heavily implanted germanium.

This paper is structured as follows. In Sec. II the experimental details are given. Cross-sectional transmission electron microscopy (XTEM) and multiple internal transmission-mode Fourier-transform infrared absorption spectroscopy (MIT-FTIR) measurements are then presented in Sec. III.

 ©2007 The American Physical Society

These results are discussed in Sec. IV to arrive at a model for the role of hydrogen in the H-induced layer exfoliation of Ge with conclusions presented in Sec. V.

## II. EXPERIMENTAL DETAILS

Double-side polished Ge(100) arsenic-doped wafers were used for this study. The resistivity was above 10 Ω $cm^{-1}$, in order to minimize free-carrier absorption during infrared absorption measurements. The substrates were implanted with 80 keV $H^+$ at an incidence angle of 7° at three doses: $2\times10^{16}$, $5\times10^{16}$, and $1\times10^{17}$ $cm^{-2}$. The wafer temperature was kept at or below room temperature as measured with a thermocouple in contact with the back surface of the substrate by cooling the back-side of the implant stage during implantation, thereby minimizing the dynamic annealing of the substrates during the implantation process. After implantation, the wafers were cut into pieces for the realization of cross-sectional transmission electron microscopy (XTEM), atomic force microscopy (AFM), and multiple internal transmission Fourier transform infrared spectroscopy (MIT-FTIR) measurements. The $40\times15\times0.5$ $mm^3$ MIT samples were beveled at 45° along the short sides, allowing radiation to enter normal to the bevel edge, and totally internally reflect on the Ge faces (the 45° internal incidence angle is much larger than the 14° critical angle for the Ge/air interface) a total of 70 times (35 times on each side). All spectra were collected with a Thermo-Nicolet spectrometer using a liquid-nitrogen cooled mercury cadmium telluride detector with a low frequency cutoff near 600 $cm^{-1}$. All implanted Ge pieces were annealed isochronally in a nitrogen ambient. Spectra were acquired following approximately 15 min isochronal annealing steps of 59, 131, 170, 221, 297, 339, 399, and 501 °C in order to follow the evolution of the chemical state of hydrogen. The temperature of the sample during anneal steps was monitored with a Sensarray thermocouple-instrumented wafer, accurate to ±0.1 °C.

## III. RESULTS

### A. TEM and AFM measurements

For the understanding of the process of H-induced layer exfoliation, the chemistry of hydrogen with Ge determined by FTIR is a key. Additionally, by transmission electron microscopy measurements it is possible to determine the density and identity of the crystallographic defects present in the crystal after ion implantation and how the defects evolve during annealing.

In Fig. 1 XTEM micrographs show both low- and high-magnification images of an as-implanted Ge sample implanted on a gas-cooled stage with $H^+$ at 80 keV to a total dose of $1\times10^{17}$ $cm^{-2}$. In Fig. 1(a), the broad distribution of the implant induced damage immediately following implant corresponds to the brighter zone, at about 600 nm from the front surface. The position and thickness matches well with the predicted distribution of H within the Ge substrate. In Fig. 1(b), a higher magnification XTEM image of the implanted region shows the presence of a large concentration of platelet defect structures parallel to the (100) planes and a smaller concentration of platelets inclined 25° with respect to the (100), parallel to the (111) planes. In the following, the platelets oriented parallel to (100) and (111) planes will be named (100) and (111) platelets. In order to discern the effect of implantation from the effect of dynamic/static annealing on the nano-structure of the Ge, X-TEM measurements were realized on implanted Ge on an un-cooled stage before and after annealing at 250 °C for 10 min. The results are illustrated in Fig. 2 by low- and high-magnification. The implant dose and energy correspond exactly to those of Fig. 1. While the dynamic temperature during implantation is higher for a sample implanted on a cooled stage than it is for an uncooled sample, the subsequent anneal of 250 °C is thought to be considerably higher than the peak temperature reached during implantation—as on the contrary exfoliation could occur during implantation. As a consequence, the images in Fig. 2 are assumed to be typical of the evolution of the defect structure in $H^+$-implanted Ge. The defect structure and distribution is shown in the low-magnification image in Fig. 2(a). The initial stages of the formation of micro-cracks at the predicted peak range of 560 nm are observed. These cracks are referred to as micro-cracks in reference to the distribution of crack lengths from 25 to 100 nm. Figure 2(b) shows the micro-cracks at increased magnification. Further inspection shows an increase in the number of (111) and (100) platelets following the 250 °C anneal. Finally, Fig. 2(c) captures the process by which the micro-cracks coalesce by jumping between (100) micro-cracks at differing depths. This process is consistent with the physical model of (100) platelets opening

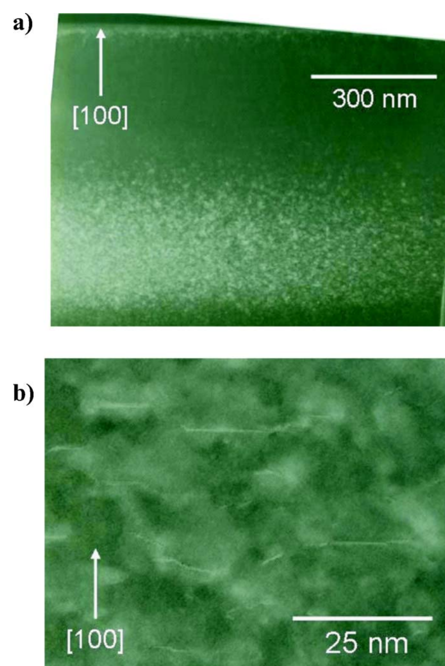


FIG. 1. (Color online) (a) An XTEM image of Ge as-implanted with 80 keV $H^+$ to a dose of $1\times10^{17}$ $cm^{-2}$ on a gas cooled stage revealing the broad damage distribution structure of Ge implanted under these conditions. (b) A high-magnification image of the heavily damaged region near the peak range of the implant showing a large concentration of (100) platelet defect structures and a smaller concentration of (111) platelets.

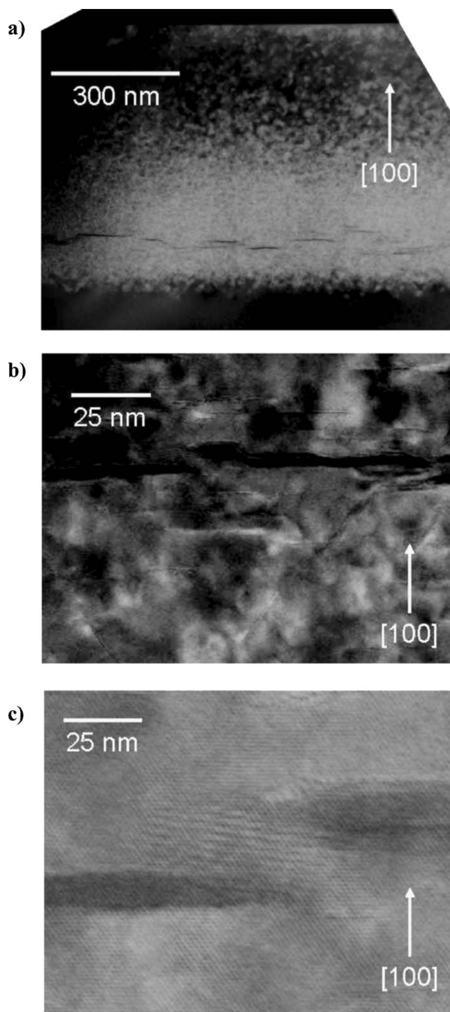


FIG. 2. (a) An XTEM image of Ge implanted with 80 keV $H^+$ to a dose of $1\times 10^{17}$ $cm^{-2}$ without active cooling following an anneal to 250 °C for 10 min. (b) A high magnification XTEM image of the micro-crack region under the same conditions presence of (100) and (111) hydrogen platelets and micro-cracks just beginning to form in the material. (c) A high-resolution XTEM image of Ge implanted with 80 keV $H^+$ to a dose of $1\times 10^{17}$ $cm^{-2}$ without active cooling following an anneal to 250 °C for 10 min under close magnification showing the coalescence of nanocracks into microcracks that eventually lead to exfoliation.

at various implantation depths to form micro-cracks. These micro-cracks are distributed in depth in the film around the range of the implant. To complete the exfoliation process, the micro-cracks ripen to form extended macro-crack structures by the joining of micro-cracks at various depths in the H-implanted region of the Ge substrate through crack-jumping along planes that otherwise would not preferentially form a cleavage plane.

To corroborate the evolution of the structural properties of the implanted Ge annealed at higher temperatures, we present some AFM measurements of the surface. While the wafer surface topology is unchanged following $H^+$ implantation, the presence of blisters at the surface can be observed by AFM once the micro-cracks start coalescing and open cavities formed. Figure 3(a) shows the development of blisters on the surface of an implanted Ge substrate annealed for 10 min at 250 °C. There is a dense coverage of small surface protrusions corresponding to blisters formed in the early stages of the exfoliation process. Following an additional 10 minute anneal at 300 °C, an AFM image shown in Fig. 3(b), it is shown that the disperse blisters have ripened into larger blisters. The ripening of the blisters provides a direct support for the physical picture suggested by the XTEM images. That is, the exfoliation process is initiated with the formation of a dense network of micro-scale cracks around the peak range of the H-implant. Upon further annealing, as seen by the crater-like structure found in Fig. 3(b), the rupture of the blister is observed, most probably due to the accumulation and further increase of the internal gas pressure of the $H_2$ inside the blister.

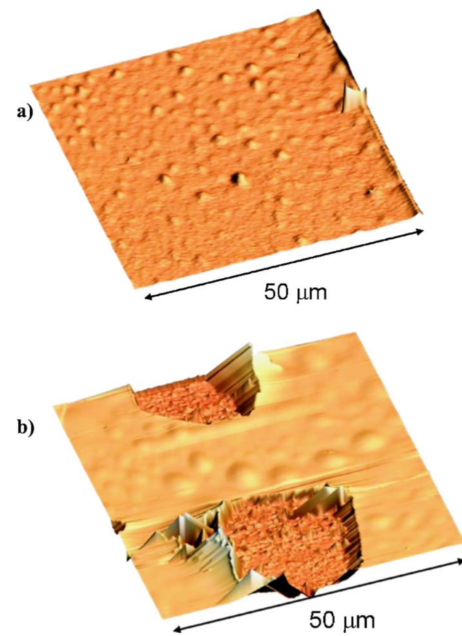


FIG. 3. (Color online) (a) A contact mode AFM image of an H-implanted Ge surface following an anneal to 250 °C for 10 min for an 80 keV $H^+$ dose of $1\times 10^{17}$ $cm^{-2}$ without active cooling. (b) A contact mode AFM image of the same surface following an anneal to 300 °C for 10 min.

XTEM and AFM analysis of $H^+$-implanted Ge have shown that implantation creates some extended defects such as platelets. These platelets become more defined and grow during annealing before the rupture of the internal cavities and exfoliation of a surface layer of the wafer. MIT-FTIR measurements presented in the next section serve to elucidate the chemical role of hydrogen in the exfoliation of $H^+$ implanted Ge.

### B. MIT-FTIR spectroscopy measurements

#### *1. Basic principles*

TEM and AFM are valuable for showing the physical phenomena that occur during the exfoliation and layer transfer of a Ge thin film in H-implantation-induced exfoliation but are not sensitive to chemical changes in the process. In

contrast, vibrational spectroscopy is best-suited to understand the chemical state and role of H in the exfoliation process, which dominate the microscopic mechanisms. Specifically, MIT-FTIR spectroscopy, performed as a function of the electric field polarization, can provide information on the orientation of Ge-H modes and/or the location of bound hydrogen. Indeed, the intensity of Ge-H modes polarized normal to the surface (or crack direction) can be greatly enhanced if the Ge-H species are located in a region of low index of refraction.[7,12] Following a simple three-layer model, the absorption of radiation upon transmission at an interface region is

$$\frac{\Delta I}{I_0}=\frac{2\pi d}{\lambda}\cdot\frac{1}{n\cdot\cos\Theta}\left[\cos^2\Theta\cdot\mathrm{Im}\,\tilde{\epsilon}+n^4\sin^2\Theta\cdot\mathrm{Im}\,\frac{-1}{\tilde{\epsilon}}\right], \tag{1}$$

where $\Theta$ is the internal angle of incidence, $d$ and $\tilde{\epsilon}$ are the effective interface thickness and dielectric function, respectively, and $n$ is the substrate index of refraction (germanium in our case). The absorption has two different contributions, the first proportional to the imaginary part of epsilon associated with absorption parallel to the interface and a second proportional to the inverse of epsilon, associated with absorption perpendicular to the interface. The ratio between the absorption of parallel and perpendicular radiation is then

$$\frac{\perp}{\parallel}=\frac{n^4\sin^2\Theta}{|\tilde{\epsilon}|^2\cos^2 a}. \tag{2}$$

For an incidence angle of 45°, the enhancement of one of the components comes from the relatively much lower index of refraction of the interfacial region. This situation occurs for hydrogen at the surface of cracks only when the fracture is well developed (i.e., when the index is close to 1) and the absolute enhancement greatly depends on the distance of the crack to the outer surface. However, in cases where the cracks are in a distance within the wavelength from the outer surface of the sample, it is also necessary to take into account the interference of the incident and reflected beam. Under these conditions, the intensity of each polarization is also proportional to the square of the electrical field components which is given by the expressions,[9]

$$|\mathbf{E}_s|^2=4E_0^2\cdot\left|\sin\Theta\cos\left(k_z\cdot\ +\frac{1}{2}\Delta\Psi\right)\right|^2, \tag{3a}$$

$$|\mathbf{E}_p|^2=E_0^2\cdot\left|\sin\Theta\cos\left(k_z\cdot z+\frac{1}{2}\Delta\Psi\right)\right|^2+E_0^2\cdot\left|\cos\Theta\cos\left(k_z\cdot z+\frac{1}{2}\Psi_p\right)\right|^2, \tag{3b}$$

$$\frac{1}{2}\Psi_p=-\arctan\frac{n^2\sqrt{n^2\sin^2\Theta-1}}{n\cdot\cos\Theta}, \tag{3c}$$

$$\frac{1}{2}\Delta\Psi=\frac{\pi}{2}-\frac{1}{2}\Psi_p, \tag{3d}$$

where $z$ is the distance of the low index region from the surface (600 nm in our case) and $\mathbf{E}$ is the electrical field, $\mathbf{k}$ the wave vector and the subindexes correspond to the different components. The comparison of spectra taken in $s$- and $p$-polarization provides the additional information necessary to distinguish the configuration and location of hydrogen at various steps of the process. From Eqs. (1)–(3) the formation of a low index layer (the cracks) would lead to an increase of absorption of the modes taken with $p$-polarization in comparison to that of $s$-polarized spectra. This enhancement does not require a large gap, as was demonstrated in the case of the bonding of two H-terminated Si wafers, where the distance between two Si surfaces is believed to be $\approx 4$ Å.[13] The most important parameter is the perfection of the lateral extend of the crack, since the IR beam is affected by the effective index of the crack. The location of neighboring cracks should be within the average crack length to insure that there is a definable average crack position with a lower index of refraction.

#### *2. Total implantation dose dependence*

The three implantation doses studied exhibit three different physical behaviors: (1) $2\times10^{16}$ cm$^{-2}$—a sub-critical dose that does not blister upon annealing; (2) $5\times10^{16}$ cm$^{-2}$—an intermediate dose that exhibits blistering only at temperatures above 500 °C; and, (3) $1\times10^{17}$ cm$^{-2}$—a high dose that leads to lower-temperature blistering. MIT-FTIR spectra of the three different implanted Ge wafers maintained at room temperature (i.e., no anneals after implantation) are compared in Fig. 4 for measurements performed both under $s$- and $p$-polarization. The spectra taken with $s$-polarization show much richer spectral details, because none of the bands are strongly enhanced. In contrast, the spectra taken with $p$-polarization are dominated by the enhancement of features associated with H located in the low density area of the material (cracks and internal surfaces), making it difficult to distinguish H located in discrete defects in the bulk (i.e., outside of the lower-index, heavily-damaged region). For this reason, the assignment of discrete defect modes at low temperature is done using spectra taken with $s$-polarization. Important additional information to positively identify discrete defect modes is obtained from temperature dependence measurements (Figs. 5–7), from which the thermal stability of the defects can be derived. Table I catalogs the dominant peaks observed in the different implant conditions as a function of temperature. The peaks present in spectra measured with both with $s$- and $p$-polarizations are indicated in parentheses. Additionally, Table I lists values reported in the literature for well-studied defect structures of hydrogen on Ge surfaces, in interstitial and vacancy defects in Ge, which is helpful to interpret the spectra and to follow the evolution of discrete and extended defects measured by MIT-FTIR in H-implanted germanium.

#### *3. Temperature dependence*

The temperature-dependence of all H-induced modes is shown for three different doses: $2\times10^{16}$ cm$^{-2}$ in Fig. 5, 5

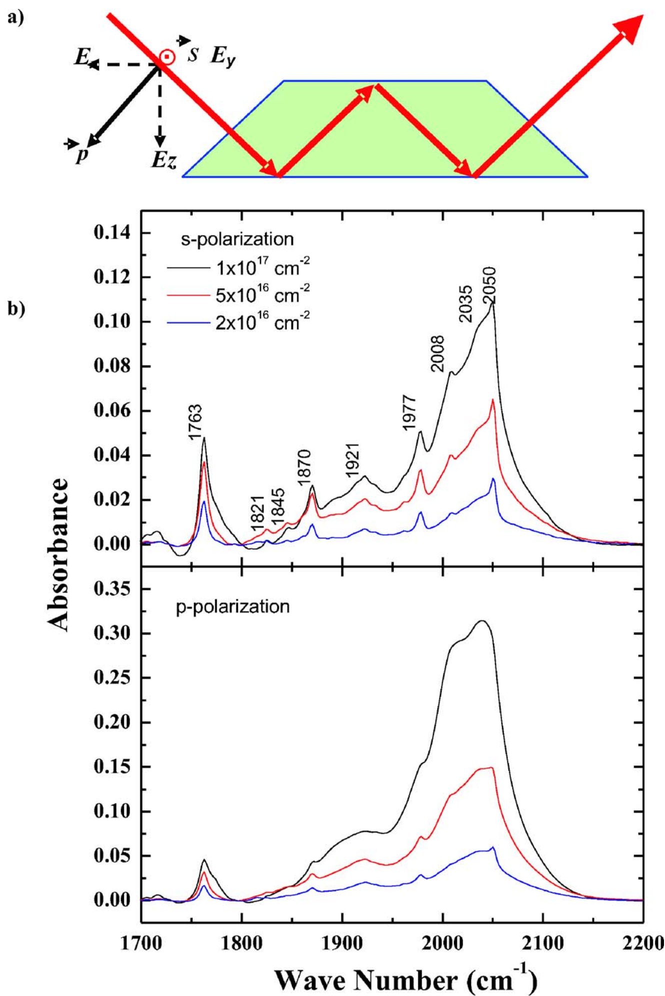


FIG. 4. (Color online) (Color online) MIT-FTIR of unannealed H-implanted samples of $2\times10^{16}$ cm$^{-2}$, $5\times10^{16}$ cm$^{-2}$, and $1\times10^{17}$ cm$^{-2}$ showing the discrete Ge-H defect modes seen in this study. The top panel shows spectra taken with *s*-polarization and the bottom panel shows spectra taken with *p*-polarization.

$\times10^{16}$ cm$^{-2}$ in Fig. 6, and $1\times10^{17}$ cm$^{-2}$ in Fig. 7. Examining the spectra taken with *s*-polarization, it appears the temperature dependence of the peaks attributed to discrete defects is consistent for all three implant conditions. For instance, features located at 1763 and 1979 cm$^{-1}$ have been associated with the Ge-$H_2^*$ defect structure. The position of these features, measured at 333 K, is close to the values reported by Nielsen *et al.* measured at 10 K for the Ge-$H_2^*$ anti-bonding (1763 cm$^{-1}$) and bond centered (1989 cm$^{-1}$) stretch modes, respectively.[14] Although there is a small discrepancy for the bond centered stretch, both modes display the same thermal evolution reported by Nielsen (e.g., they vanish after a 443 K anneal, which compares favorably to 438 K reported by Nielsen *et al.*). Additional support for this assignment is the observation of a feature with the same temperature dependence at 763 cm$^{-1}$ very close to the frequency of 765 cm$^{-1}$ reported for the Ge-$H_2^*$ bending mode.[15] The small differences with the values reported by Nielsen *et al.* are most likely due to the measurement temperature.

In addition to the frequencies assigned to the $H_2^*$ stretch modes, there are at least seven other modes in the range from 1700–2200 cm$^{-1}$. Among them, the feature at 1870 cm$^{-1}$ is near the frequency of the stretch mode of the dihydrogenated self-interstitial, $IH_2$, at 1880 cm$^{-1}$ reported by Nielsen *et al.* The temperature behavior of this defect also corroborates this assignment with the feature disappearing by 221 °C, slightly below the literature reported value of 240 °C.[14] The strong feature located at 2050 cm$^{-1}$ is near the reported value of the $VH_4$ defect at 2061.5 cm$^{-1}$, but also close to the stretching frequency of the germanium trihydride $GeH_3$. This feature is seen to vanish between anneals of 297 and 339 °C, very close to the report by Nielsen *et al.* in which the feature attributed to the $VH_4$ defect was seen to vanish at 317 °C. As it will be discussed later, this feature constitutes a prominent contribution appearing after annealing that may be correlated to the formation of internal surfaces and subsequent micro-cracks.

The mode at 2008 cm$^{-1}$ observed with *s*-polarization is present for all implantation doses at room temperature and remains stable up to ≈365 °C (it disappears abruptly between 339 and 399 °C). The attribution of this mode is more controversial. Its thermal dependence and the fact that it does not exhibit any enhancement when measuring the absorption under *p*-polarization suggest that it can be assigned to a discrete defect structure that contributes molecular hydrogen to the exfoliation process and might form a precursor mode. As the mono-vacancy $VH_2$ has already been attributed to the peak present at 1979 cm$^{-1}$, one possible assignment for this peak would be the $V_2H_6$ defect with a mode reported at 2014.9 cm$^{-1}$,[8] which has been shown to be unstable above 347 °C. The ≈7 cm$^{-1}$ discrepancy could be due to strain in the Ge itself or to interaction between H in opposite side of the vacancy, which would be expected for larger vacancies ($V_nH_{n+4}$, $n>2$). Since the dihydride mode on Ge(100) is at 2020 cm$^{-1}$, it is likely that the spectral region between 1015 and 2020 cm$^{-1}$ encompasses modes of larger vacancies. Interaction between opposite surfaces of such large vacancies does lead to a red shift. For instance, in the case dihydride on Ge(100) surfaces, a shift towards lower wavenumbers occurs when the hydrogen is located in internal hydrogen terminated surfaces, due to both the interaction between the close hydrogen atoms and opposite surfaces.[16,17] This assignment of this mode would also explain its enhancement in spectra measured with *p*-polarization, and its red shift during annealing. The remaining weak modes observed in the 1700–2200 cm$^{-1}$ frequency range at room temperature cannot be assigned at present, but are assumed to correspond to hydrogen-decorated interstitials and vacancies induced during the implantation of the Ge substrate. Additionally, there is a broad background in this region similar to (although not as intense as) a broad feature observed in Si and assigned to a distribution of multi-vacancy defects of the form $V_xH_y$ and hydrogenated self-interstitials of the form $I_xH_y$.[1] A possible explanation for the difference between the background intensity in the present study and the Si-H study is that Ge would suffer less lattice damage following implant due to the larger mass of the Ge atom.

Figures 5(a) and 5(b) show the evolution of the spectra taken in both *s*- and *p*-polarizations, respectively, as a function of isochronal anneal temperature for a sub-critical dose of $2\times10^{16}$ cm$^{-2}$. The spectra in Fig. 5(a) best show the

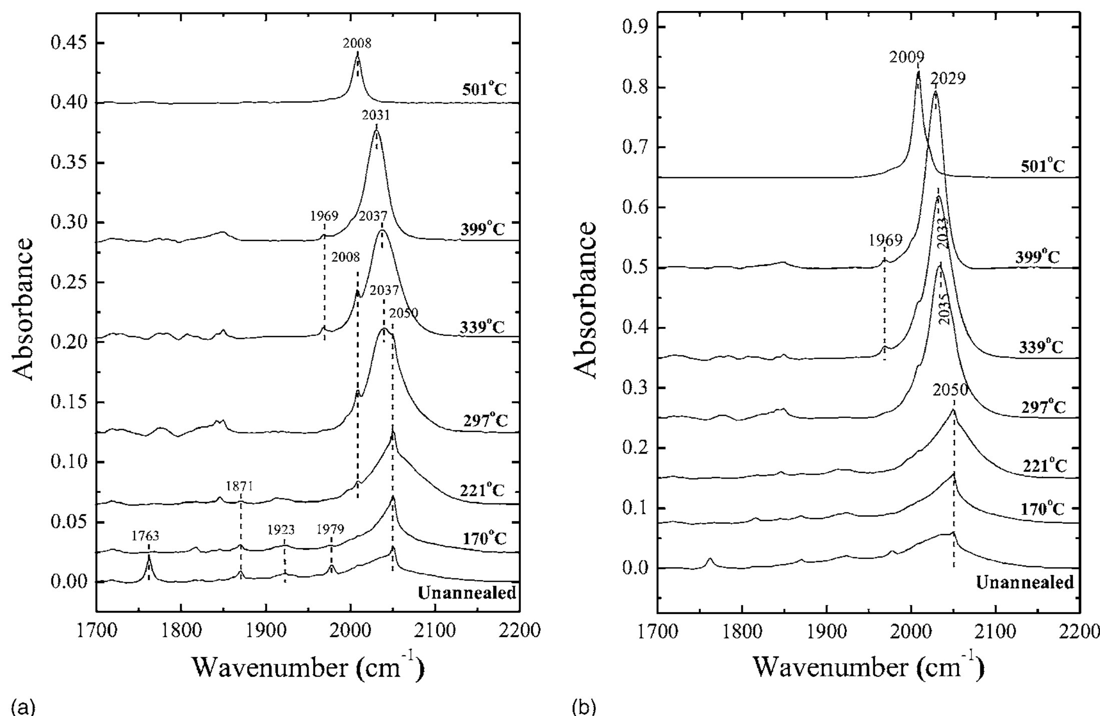


FIG. 5. (a) MIT-FTIR spectra taken with *s*-polarization for $2\times10^{16}$ cm$^{-2}$ implanted Ge as a function of the isochronal annealing temperature. (b) MIT-FTIR spectra taken with *p*-polarization for $2\times10^{16}$ cm$^{-2}$ implanted Ge as a function of the isochronal annealing temperature.

modes associated with the dominant discrete defect modes removed by relatively low temperature anneals. At temperatures above 170 °C the dominant modes are all located in the 1950–2100 cm$^{-1}$ range, which encompasses the vacancy-hydrogen defect modes as well as extended surfaces. Upon annealing, the features in the 1950–2100 cm$^{-1}$ range sharpen and evolve, with the disappearance (or red shift) of the 2050 cm$^{-1}$ mode into a single peak with greatly reduced integrated intensity at 2008 cm$^{-1}$.

The weak features seen in the 1700–1900 cm$^{-1}$ range after annealing at 297, 339, and 399 °C are difficult to assign unambiguously because they overlap partially with contamination features observed after implantation and also after annealing.[18] After subtracting strong bands attributed to contamination in this region, it is not reliable to attempt to assign the residual peaks to any Ge-H structure, particularly when none have been reported in the literature.

The spectra in Fig. 5(b) taken with *p*-polarization show the evolution of the bands that are clearly enhanced. As was previously noted, these enhanced bands dominate the spectrum and make it difficult to study Ge-H modes that are not enhanced (e.g., residing outside of the internal cracks or with a polarization parallel to the surface). In Fig. 6(b) the spectrum taken with -polarization for the unannealed sample shows minimal enhancement of the 2050 cm$^{-1}$ mode tentatively attributed to the $VH_4$ defect. After annealing to 221 °C the 2050 cm$^{-1}$ band is strengthened and broadened. However, at 297 °C a strong mode at 2035 cm$^{-1}$ develops at the expense of the 2050 cm$^{-1}$ mode. This indicates that the low refractive index region of the implanted Ge is becoming better defined and that the feature being enhanced is a major constituent of that region with a strong *z*-axis dipole. For anneals of 339 and 399 °C the enhanced feature shifts downward, and finally at 501 °C the dominant feature is greatly reduced in intensity and is found at 2009 cm$^{-1}$. This spectral evolution is in good agreement with results previously obtained by Stein *et al.* for hydrogen implanted Ge in the absence of internal voids in the Ge.[19]

The evolution of Ge-H stretch modes discussed above is associated with germanium implanted with a dose under the threshold of exfoliation. We are going now to analyze a germanium implanted at the threshold dose ($5\times10^{16}$ cm$^{-2}$). The use of a dose close to the exfoliation threshold allows the observation of the exfoliation in a more gradual way. The spectra in Figs. 6(a) and 6(b) show the corresponding evolution of the spectra taken with *s*- and *p*-polarization, respectively. As with the $2\times10^{16}$ cm$^{-2}$ sample, the mode at 2050 cm$^{-1}$ dominates the spectrum up to 221 °C. However, in contrast to the case of $2\times10^{16}$ cm$^{-2}$ implantation dose, there is a strong band in the unannealed spectrum at 2008 cm$^{-1}$ attributed to the dihydride present at extended internal surfaces that continues to grow through 339 °C. Following an annealing at 399 °C new features are observed. The dominant spectral feature is now located at 2025 cm$^{-1}$, but there are several modes at lower frequencies, including modes at 2000, 1990, and 1969 cm$^{-1}$. The slight shoulder at 1990 cm$^{-1}$ increases in intensity to become the dominant feature at 501 °C. This is once again shifted by 10 cm$^{-1}$ from the asymmetric stretch of the Ge(100) monohydride terminated surface reported by Chabal, but the shift can again be attributed to the fact that hydrogen is located in

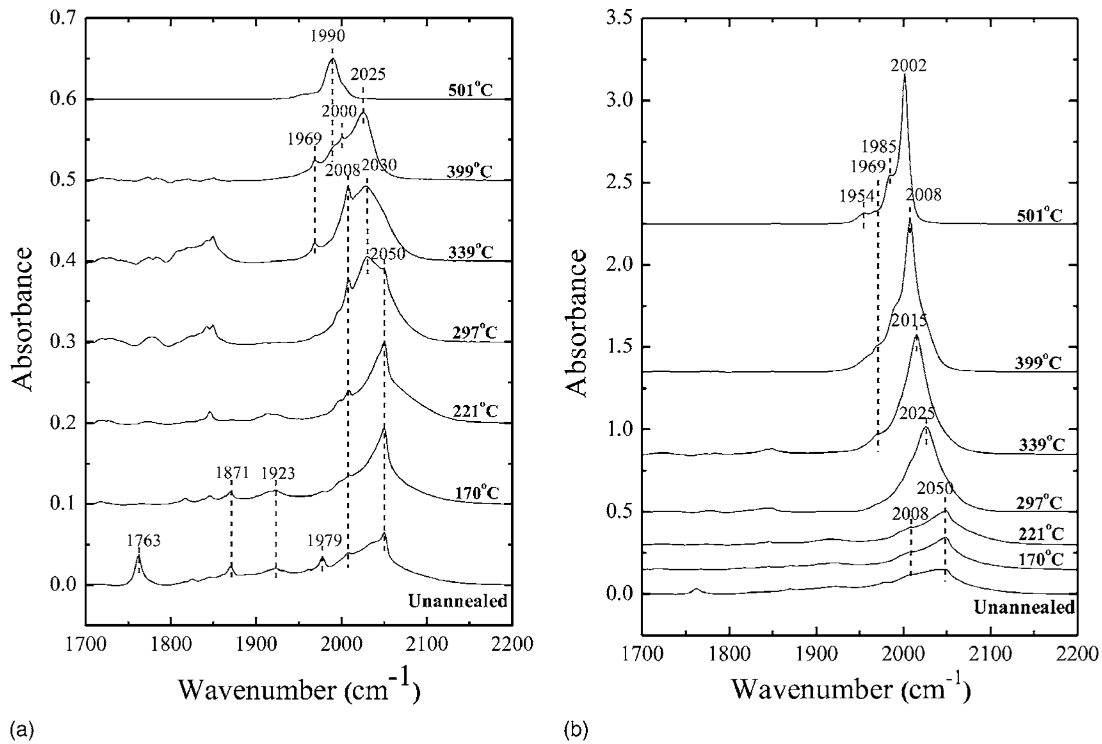


FIG. 6. (a) MIT-FTIR spectra taken with $s$-polarization for $5\times10^{16}$ cm$^{-2}$ implanted Ge as a function of the isochronal annealing temperature. (b) MIT-FTIR spectra taken with $p$-polarization for $5\times10^{16}$ cm$^{-2}$ implanted Ge as a function of the isochronal annealing temperature.

internal and not open surfaces.[20] Following the 501 °C anneal there remains a slight shoulder extending to $\approx$1950 cm$^{-1}$. This shoulder encompasses the reported values of 1978 cm$^{-1}$ for the Ge(111) surface mono-hydride.[9] Thus, these data provide evidence of the presence of (100) and (111) internal surfaces at 501 °C.

In Fig. 6(b), the spectra taken with $p$-polarization, critical steps in the evolution of the Ge-H structure necessary for exfoliation are again observed by the increase in the enhancement. The main characteristics of these measurements are the relatively simple nature of the spectra (only one or two peaks) and relatively little enhancement from the as-implanted condition through a 221 °C anneal. Upon annealing to 297 °C there is an onset of enhancement with a strong peak at 2025 cm$^{-1}$. Following the 339 °C anneal, the enhanced peak continues to shift downward to 2015 cm$^{-1}$. The sample annealed to 399 °C shows a further shift in the dominant peak down to 2008 cm$^{-1}$ accompanied by increased spectral detail in the low-frequency shoulder of this peak, which at this temperature appears to have contributions from modes at 1969 and 2000 cm$^{-1}$. Both of these features were also observed in the spectrum taken with $s$-polarization, suggesting that they are modes with a parallel dipole. Finally, upon annealing to 500 °C, a temperature at which the onset of blistering is observed but at which exfoliation has not yet occurred, the enhanced peak shifts further to 2002 cm$^{-1}$ and now has clearly distinguishable shoulder features at lower frequencies due to peaks estimated to be located at 1954, 1969, and 1985 cm$^{-1}$. The symmetric stretch mode of the Ge(100) surface monohydride being reported in a much lower frequency of 1991 cm$^{-1}$, we attribute the strong feature shifting from 2025 to 2002 cm$^{-1}$ to the evolution of isolated trihydrides on Ge (100) surfaces to the accumulation forming germanium dihydrides.[21,22] The shoulder at 1985 cm$^{-1}$ is near the Ge(111) surface monohydride value seen by Stein *et al.* of 1978 cm$^{-1}$. Furthermore, it is consistent with the physical picture of the ripening of micro-cracks into an extended crack structure by fractures along the higher index planes such as the (111) separating the micro-cracks that lie primarily on the Ge(100) plane.

The MIT-FTIR spectra for the low-temperature-blistering condition $1\times10^{17}$ cm$^{-2}$ taken with both $s$- and $p$-polarizations as a function of temperature are shown in Figs. 7(a) and 7(b), respectively. The spectrum taken with $s$-polarization for the unannealed sample shows the dominant discrete features that were previously noted. As with the 2 and $5\times10^{16}$ cm$^{-2}$ samples, the mode at 2050 cm$^{-1}$ dominates the spectrum up to 221 °C. However, in contrast to the case of lower implantation doses, there is a strong band in the unannealed spectrum at 2008 cm$^{-1}$ attributed to germanium dihydrides in extended internal surfaces, that continues to grow through 339 °C. At 297 °C a strong peak forms at 2032 cm$^{-1}$, while the peak at 2050 cm$^{-1}$ is significantly diminished. Just prior to blistering, following an anneal to 339 °C, the peak at 2032 cm$^{-1}$ shifts to 2027 cm$^{-1}$ while a peak at 1969 cm$^{-1}$ appears in the spectrum. At 399 °C, exfoliation has occurred and the Ge-H modes in the spectrum originate from hydrogen residing below the cleavage plane and on free surfaces created by the blister process. In the spectrum taken with $s$-polarization in Fig. 7(a) there is still a

TABLE I. Peak location as a function of temperature for peaks in the 1900–2100 $cm^{-1}$ for $2\times10^{16}$, $5\times10^{16}$ and $1\times10^{17}$ $cm^{-2}$. When the peaks measured with *p*-polarization are shifted to other frequencies, these are indicated between parentheses. The peaks featured in MIT-FTIR spectra that show strong enhancement are indicated with an asterisk. Attribution of the measured peaks according to the literature reported values for discrete defect and extended surface modes of hydrogen in Ge.

| Temperature | $2\times10^{16}$–Subcritical | $5\times10^{16}$ | $1\times10^{17}$ | Peak explanation |
|---|---|---|---|---|
| Unannealed | 1763 | 1763 | 1763 | 1763 $cm^{-1}$: anti-bonding, stretch modes of Ge-$H_2^*$ at 10 K |
| | 1979 | 1979 | 1979 | 1979: (100) Monohydride asymmetric stretch/$VH_2$ |
| | 2008 | 2008 | 2008 | Hydrogenated Ge vacancy |
| | 2050 | 2050 | 2050 (2038) | $VH_4$ or similar |
| 170 | | | 1996 | $VH_2$ (1993) |
| | 2008 | 2008 | 2008 | Hydrogenated Ge vacancy |
| | 2050 | 2050 | 2050 (2046) | $VH_4$ |
| 221 | | 1996 | 1996 | $VH_2$ (1993) |
| | 2008 | 2008 | 2008 | Hydrogenated Ge vacancy |
| | 2050 | 2050 | 2050 (2046) | $VH_4$ |
| 297 | | 1996 | 1996 | $VH_2$ (1993) |
| | 2008 | 2008 | 2008 | Hydrogenated Ge vacancy |
| | 2040* (2035) | 2030* (2027) | 2033* (2015) | $V_2H_6$ |
| | 2050 | 2050 | 2050 | $VH_4$/trihydride |
| 339 | 1969 | 1969 | 1969 | 1969: (111) monohydride stretch |
| | | 1996 | | 1996: (100) monohydride asymmetric stretch |
| | 2008 | | 2008 | Hydrogenated Ge vacancy |
| | 2038* (2033) | 2029* (2015) | 2027* | $V_2H_6$ |
| 399 | 1969 | 1969 | 1972 | 1969: (111) monohydride stretch |
| | | 1990 | 1992 | 1996: (monohydride asymmetric stretch) |
| | | 2001 | | Hydrogenated Ge vacancy/collective dihydride stretch |
| | 2031* (2033) | 2025* (2008) | 2027 | $V_2H_6$ |
| 501 | | 1962 (1957) | | 1969: (111) monohydride stretch |
| | | 1980 (1970) | | 1980: (100) monohydride asymmetric stretch |
| | | 1990 (1986) | | 1990: (100) monohydride asymmetric stretch |
| | 2008+(2021) | 2002 | | Hydrogenated Ge vacancy/collective dihydride stretch |

strong contribution at 2027 $cm^{-1}$. However, the contribution at 2008 $cm^{-1}$ is no longer discernible, which agrees with the hypothesis that this mode corresponds to the hydrides present at the opening internal surfaces that contribute to the exfoliation process. A peak at 1991 $cm^{-1}$ has formed, which is near the value of 1979 $cm^{-1}$ reported by Chabal for the asymmetric stretch-mode of Ge(100) monohydride.[10] This mode is polarized parallel to the surface and should therefore be observed with *s*-polarization for internal surfaces parallel to the surface, which should be observed in the -polarized spectra due to the orientation of the dipole for this mode.

The spectrum taken with *p*-polarization in Fig. 7(b) shows relatively little spectral detail due to the strong enhancement seen even prior to annealing. There is a slight shift of the dominant band at 2046 $cm^{-1}$, relative to the dominant feature at 2050 $cm^{-1}$ observed for samples implanted to $2\times10^{16}$ and $5\times10^{16}$ $cm^{-2}$. Additionally, there is a broad shoulder toward lower frequencies that is suggestive of a peak near 2008 $cm^{-1}$ as was observed in the spectrum taken with *s*-polarization for the unannealed sample. Annealing to 221 °C causes only a slight change in the peak profile along with the loss of the Ge-$H_2^*$ features at 1763 and 1979 $cm^{-1}$. Upon annealing to 297 °C, there is a dramatic increase in the enhancement indicating the onset of blistering accompanied by a shift of the dominant peak to 2031 $cm^{-1}$. This dominant peak must be related to an internal structure with substantial *z*-component dipole. Such a H-decorated internal structure is, therefore, a precursor to the exfoliation of the thin film. Upon annealing to 339 °C there is further enhancement and sharpening of the major peak, which has now shifted down to 2008 $cm^{-1}$. Finally, following a 399 °C annealing, the film is exfoliated and, as one would expect, the enhancement of the spectrum is no longer observed. In addition to the now diminished peak at 2008 $cm^{-1}$, there are clearly distinguishable shoulders at 1992 and 2027 $cm^{-1}$ that were likely present in the spectrum taken following the 339 °C anneal but remained unobserved due to the peak enhancement at 2008 $cm^{-1}$ (Fig. 8).

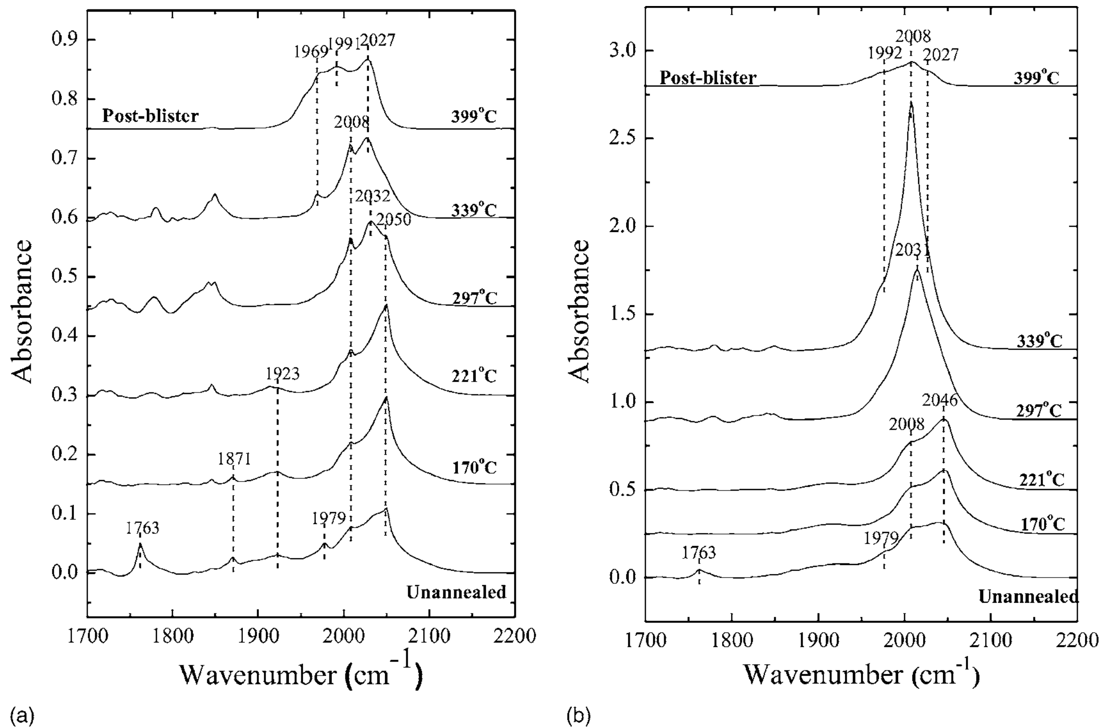


FIG. 7. (a) MIT-FTIR spectra taken with $s$-polarization for $1\times10^{16}$ cm$^{-2}$ implanted Ge as a function of the isochronal annealing temperature. (b) MIT-FTIR spectra taken with $p$-polarization for $5\times10^{16}$ cm$^{-2}$ implanted Ge as a function of the isochronal annealing temperature. The spectra for 399 °C for both polarizations is taken following exfoliation of the implanted Ge layer.

## IV. DISCUSSION

In the preceding section, the essential elements of the exfoliation process in germanium were highlighted and discussed separately for the three different implantation doses. We now can combine these elements to first propose a coherent mechanism for the hydrogen induced exfoliation of germanium and then compare it with the mechanism developed elsewhere for silicon.[7,23]

The first important observation is that after implantation hydrogen is located mainly in defect structures such as hydrogenated vacancies with different degrees of hydrogenation. The dominant features in the spectrum taken with $s$-polarization are at 1979, 2008, and 2050 cm$^{-1}$, which are respectively consistent with interstitial defects and mono- and multi-hydrogenated vacancies. Following annealing, poorly hydrogenated defects tend to disappear in favor of more highly hydrogenated defects and internal planes. Interesting is the evolution of the peaks located at the highest frequencies, from 2008 to 2050 cm$^{-1}$. The feature at 2050 cm$^{-1}$ is attributed to the hydrogenated vacancy $VH_4$, while the feature at 2027 cm$^{-1}$ is attributed to agglomerated defect structures ($V_2H_6$ and $V_nH_{n+4}$) that are precursors to blistering, as will be discussed below, and are still present in the substrate below the exfoliated region. The spectrum taken with $p$-polarization has a strongly enhanced peak at 2008 cm$^{-1}$ that slightly remains following exfoliation only in the sample implanted with the highest dose. In the same sample and following exfoliation at 399 °C, there is a broad tail toward 1950 cm$^{-1}$ that is consistent with the presence of Ge(111) surface monohydride modes.[9] The mechanism described above is similar to the case of silicon, but there are some differences. In both cases there is a formation and transformation of hydrogenated vacancy species into extended internal surfaces. However, the nature of the vacancies contributing to the formation of the extended internal defects and the nature of hydrogen passivation inside the cavities are different. In the case of silicon it seems that $VH_2$ vacancies are the main contributors to the exfoliation, while in the case of germanium the formation of larger vacancies (e.g., $V_2H_6$ and $V_nH_{n+4}$) appears to be the key metastable

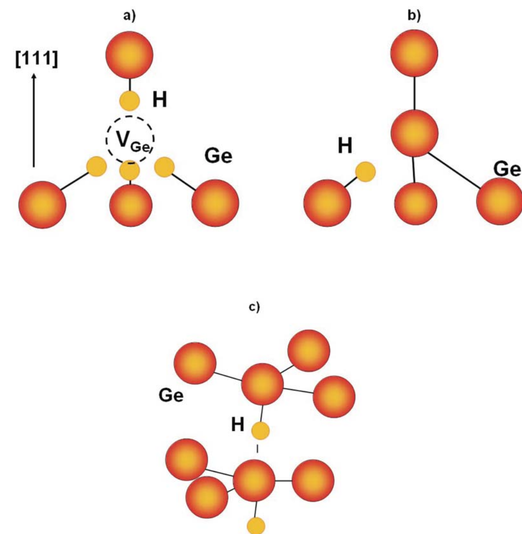


FIG. 8. (Color online) Basic schematics of the hydrogen in the (a) vacancy, (b) interstitial, and (c) $H_2^*$ configurations.

intermediate. Moreover, in silicon, cavities are passivated by monohydrides while in the case of germanium cavities seem to be passivated both by monohydrides and dihydrides. We believe that these results may explain why higher doses are needed for exfoliation of Ge compared to Si and point to subtle but important differences in these two otherwise similar materials.

## V. CONCLUSIONS

Based upon the physical and chemical observations made by TEM, AFM, and MIT-FTIR, a qualitative understanding of the H-induced layer transfer process in Ge has been achieved. Similarly to the case of Si, defects are formed in the germanium structure upon H-implantation, which trap hydrogen in a large variety of modes assigned by FTIR spectroscopy to Ge-$H_2^*$, $V_2H_6$, and $V_nH_{n+4}$. Upon annealing, some of these structures are lost and the hydrogen therein is free to move through diffusion to more stable configurations such as internal (100) and (111) surfaces, which act as the nucleation points for internal cavities and platelets. This is further supported by XTEM observation of (100)-oriented defect structures typical of platelets immediately following implantation and by the possible spectroscopic signal at 1996 $cm^{-1}$ assigned to (100) platelet structures. Upon sufficient annealing micro-cracks form along the same orientation in the crystal, lying predominantly along the (100) plane, as observed by XTEM. Simultaneously, vibrational frequencies associated with Ge(100) surface mono- and dihydride appear in the FTIR spectra, indicating that hydrogen provides a termination species for the internal blister structures. These micro-cracks and their agglomerated precursors serve as points for the coalescence of $H_2$ and the development of internal pressure sufficient to break bonds and extend the internal fracture laterally. Upon ripening of the micro-cracks into supercritical radius internal surfaces, blisters pop-up and lead to the exfoliation of the thin Ge film. This work, therefore, confirms that the exfoliation process in Ge is similar to that in Si, despite differences in Ge-H bond strength and Ge chemical activity.

## ACKNOWLEDGMENT

The authors kindly acknowledge Martin M. Frank for helpful discussions and insights in the MIT experiments.

[1] M. Bruel, Electron. Lett. **31**, 1201 (1995).
[2] U. Goesele and Q. Tong, Annu. Rev. Mater. Sci. **28**, 215 (1998).
[3] J. Zahler, C. Ahn, S. Zaghi, H. A. Atwater, C. Chu, and P. Iles, Thin Solid Films **403**, 558 (2002).
[4] A. Fontcuberta i Morral, J. Zahler, and H. A. Atwater, Appl. Phys. Lett. **83**, 5413 (2003).
[5] I. Radu, I. Szafraniak, R. Scholz, M. Alexe, and U. Goesele, J. Appl. Phys. **94**, 7820 (2003).
[6] S. Hayashi, D. Bruno, and M. Goorsky, Appl. Phys. Lett. **85**, 236 (2004).
[7] M. Weldon, V. Marsico, Y. Chabal, A. Agarwal, D. Eaglesham, J. Sapjeta, W. Brown, D. Jacobson, Y. Caudano, S. Christman *et al.*, J. Vac. Sci. Technol. B **15**, 1065 (1997).
[8] M. Weldon, M. Collot, Y. Chabal, V. Venezia, A. Agarwal, T. Haynes, D. Eaglesham, S. Christman, and E. Chaban, Appl. Phys. Lett. **73**, 3721 (1998).
[9] A. Fontcuberta i Morral, J. Zahler, M. Griggs, H. A. Atwater, and Y. Chabal, Phys. Rev. B **72**, 085219 (2005).
[10] S. Myers, H. Stein, and D. Follstaedt, Phys. Rev. B **51**, 9742 (1995).
[11] S. Myers, D. Follstaedt, G. Petersen, C. Seager, H. Stein, and W. Wampler, Nucl. Instrum. Methods Phys. Res. B **106**, 379 (1995).
[12] Y. Chabal, Surf. Sci. Rep. **8**, 211 (1988).
[13] M. Weldon, Y. Chabal, S. Christman, E. Chaban, L. Feldman, and D. Hamann, J. Vac. Sci. Technol. B **14**(4), 3095 (1996).
[14] M. Budde, B. Nielsen, P. Leary, J. Goss, R. Jones, P. Briddon, S. Oberg, and S. Breuer, Phys. Rev. B **57**, 4397 (1998).
[15] M. Budde, B. Nielsen, R. Jones, J. Goss, and S. Oberg, Phys. Rev. B **54**, 5485 (1996).
[16] D. Feijoo, Y. Chabal, and S. Christman, Appl. Phys. Lett. **65**, 2548 (1994).
[17] Y. Chabal, M. Hines, and D. Feijoo, J. Vac. Sci. Technol. A **13**, 1719 (1995).
[18] Following implantation visual and spectroscopic evidence indicated the presence of surface oxidation due to increased base pressure near the sample in the gas cooled implantation stage. Following implantation, there is a large amount of absorption in the region where one would expect the O-H stretch of water to be observed. Additionally, absorption in the Ge-O region near 1000 cm? further corroborates the presence of a water saturated oxide. By etching the sample in 10 p.c. HF for approximately 30 min, this contamination was removed and a subsequent spectrum shows little or no absorption in these regions. The contribution of contamination due to annealing was determined by the observation of peak growth in both the water and germanium oxide modes upon annealing.
[19] S. Myers, H. Stein, and D. Follstaedt, Phys. Rev. B **51**, 9742 (1995).
[20] Y. Chabal, Surf. Sci. **168**, 594 (1986).
[21] F. Maroun, F. Ozanam, and J. Chazalviel, Chem. Phys. Lett. **292**, 493 (1999).
[22] S. Rivillon, Y. Chabal, F. Amy, and A. Kahn, Appl. Phys. Lett. **87**, 253101 (2005).
[23] M. Weldon, M. Collot, Y. Chabal, V. Venezia, A. Agarwal, T. Haynes, D. Eaglesham, S. Christman, and E. Chaban, Appl. Phys. Lett. **73**, 3721 (1998).